Spatial analysis of trend in extreme daily rainfall in southern France

Juliette Blanchet, Gilles Molinié, Julien Touati

Spatial analysis of trend in extreme daily rainfall in southern France

Juliette Blanchet *[1,2], Gilles Molinié[1], and Julien Touati[1]

[1]Univ. Grenoble Alpes, LTHE, F-38000 Grenoble, France

[2]CNRS, LTHE, F-38000 Grenoble, France

February 12, 2016

Abstract

This paper makes a regional evaluation of trend in yearly maxima of daily rainfall in southern France, both at point and spatial scales on a regular grid of $8 \times 8\text{km}^2$. In order to filter out the high variability of rainfall maxima, the current analysis is based on a non-stationary GEV modeling in which the location parameter is allowed to vary with time. Three non-stationary models are considered for each series of maxima by constraining the location parameter to vary either linearly, linearly after a given date or linearly up to a final date. Statistical criteria are used to compare these models and select the best starting or final point of putative trends. The analysis shows that, at regional scale, the best distribution of maxima involves a linear trend starting in year 1985 and that this trend is significant in half the region, including most of the mountain ranges and part of the Rhône valley. Increases in yearly maxima are considerable since they reach up more than 60 mm/day in 20 years, which is more than 40% of the average maximum in this area.

1 Introduction

An exceptional number of heavy rainfall and flooding events occurred in 2014. A storm struck the Brittany region of western France at the end of December 2013 and the subsequent flood lasted until mid January 2014. In February, the Ulla storm passed over Brittany and flooded again along its way to Great Britain. Southeastern Europe (Serbia, Croatia, Romania) faced flood events in May, the Basque county (southwestern France) in July, northeastern France in August, the eastern shore of Spain and southern France in Fall and then Italy in November and

*juliette.blanchet@ujf-grenoble.fr

December. Is this sudden large number of floods due to natural climate variability, or is it a consequence of anthropogenic climate change?

Already at the end of the 70's, [Charney et al., 1979] envisioned the possible impact of human activity on climate at a global scale. Then the successive Assessment Reports (AR) of IPCC strengthened the evidence of a global change whose main manifestation is an increase in global temperature. [IPCC, 2013] states that global surface temperature has increased by about 0.9°C between 1880 and 2012, with a particularly marked warming since the 1970s. Analyzing climate change impact on precipitation is more arduous, first because precipitation is highly variable and second because its change in recent past shows multiple facets ([Alpert et al., 2002]). Mean precipitation increased under the 40°N area in Europe, Russia, United States, South America and the center of Australia between 1951 and 2010, whereas it decreased over the same period in Eastern Asia, Southern Europe and most of Africa ([IPCC, 2013]). Then what about extreme precipitation? Some studies support a causal relationship. [Planton et al., 2008], working in the context of CMIP3 simulations, shows the impact of global warming on the French climate and specifically on precipitation extremes at the end of the century. However, according to [Gallant et al., 2013], this conclusion is not supported by the recent climate records at European scale. Indeed, despite a clear warming signal in continental indices of temperature, no significant trend is detected in continental indices of precipitation. Is there any trend hidden by the spatial integration of [Gallant et al., 2013]? Focusing on point rainfall measurements, several studies illustrate the spatial variability of extreme precipitation trends over these last decades. [Haylock and Goodess, 2004] reports an increase in the occurrence of heavy rainfall days (defined as the number of days with daily amounts above the 90th percentile) in northern Europe during winter, while it decreases in southern Europe. [Zolina, 2014] considers the length of heavy rainfall period as an extreme rainfall characteristics and shows that trends in these lengths are highly variable across Germany. [Schmidli and Frei, 2005] uses 12 extreme precipitation indices to characterize swiss rainfall records and finds again highly variable trends. In particular, the number of heavy rainfall days in winter decreases in northeastern Switzerland while it increases in the Southeast. [Toreti et al., 2010] shows that trend in the probability of observing an extreme event varies along the mediterranean coast, with a significant negative trends found in 6 of the 20 studied costal sites. Still in the mediterranean region, [Alpert et al., 2002] shows that extreme daily rainfall from Spain to Israel increased between 1951 and 1990 in spite of the fact that total rainfall generally decreased.

Regarding recent trends in extreme precipitation in southern France, [Norrant and Douguédroit, 2004] finds an increase in the 95th percentile of daily and monthly rainfall, however the inter-annual variability of the 95th percentile suggests that this is only due to the occurrence of few high

values at the beginning of the study period. Analysing regional trends in monthly and annual maximum series of precipitation in seven homogeneous climatological zones in southern France, [Pujol et al., 2007b] finds a significant increase in both annual and monthly maxima in October in the southern part of the Massif Central and a decrease in March and an increase in April in the Langedoc-Roussillon. [Pujol et al., 2007a] studies the regional evolution of daily peaks-over-threshold records in the same climatological zones and finds an increase of the occurrence and intensity of extreme daily rainfall in the southern part of the Massif Central, as well as an increase in the intensity of extreme rainfall in the Languedoc-Roussillon. Focusing on the southern region including the Cévennes-Vivarais mountain range prone to flash flood events, [Tramblay et al., 2013] shows in a peaks-over-threshold approach that a slight increase in the number of the most extreme rainfall events are observed since 1980, however no significant trend is detected with a Mann-Kendall test, neither in the event magnitudes nor in the number of occurrences per year. Still in the same region, [Tramblay et al., 2011] shows that time is a valid covariate for modelling peaks-over-threshold intensity, indicating an increasing trend in the magnitude of heavy rainfall events between 1958 and 2008. [Soubeyroux et al., 2015] finds local upward trends in annual maxima of daily precipitation in the french Mediterannean area with a Mann-Kendall test, however this increase is usually not significant. Finally studying seasonal maxima of daily precipitation in the Cévennes-Vivarais range, [Vautard et al., 2015] finds local upward trends with a median increase of about 5% per decade but few of the local trends are significant.

Clearly the variety of methodologies is a source of difficulty for summarizing the results on this topic. Two main approaches are usually undertaken. The first one is based on climate indices ([Karl et al., 1996]). The usual methodology is to define a bench of indices that are relevant for the studied region and to estimate changes in each of them by fitting regression models (e.g. [Frich et al., 2002], [Klein Tank and Können, 2003], [Zolina et al., 2008], [Alexander et al., 2006],[Karl et al., 1996],[Zhang et al., 2011]), or by comparing empirical probability density functions for various periods (e.g. [Alexander et al., 2006]). ETCCDI (Expert Team on Climate Change Detection, Monitoring and Indices) recommends the use of 27 indices, among which 11 are related to precipitation and usually describe 'moderate extremes' typically occurring several times a year ([Zhang et al., 2011]). This wide spectrum of indices intends to cope implicitly with the great variety of rainfall regimes that can result from precipitation interacting with air dynamics ([Schertzer and Lovejoy, 1987, Gupta and Waymire, 1979, Fabry, 1996, Fraedrich and Larnder, 1993]). There are as many random variables characterizing the rain intensity as there are spatial and temporal resolutions, i.e. an infinity. The approach by indices chooses to summarize these many random variables by few statistics, but then part

of the information on the random variables is lost.

The second set of approaches focuses on the heaviest rainfalls but fully characterized them by modeling their probability density function. These approaches are linked to the statistical theory of extreme values. The current study focuses on annual maxima (so-called "block-maxima approach") and models them with the so-called Generalized Extreme Value (GEV) distribution ([Coles, 2001]). This approach shows the advantage of being scale-independent: whatever the temporal and spatial scales of precipitations at hand, extreme value theory insures that the right distribution to be used is the GEV distribution (whose parameters, of course, are expected to vary from one scale to another, see [Blanchet et al., 2015]). Thus the same theoretical framework can be used for analyzing precipitations at different scales. This is particularly interesting for rainfall since rainfall severity depends on the duration and spatial extension of the events ([Ramos et al., 2005, Molinié et al., 2012, Ceresetti et al., 2010]). This is also particularly convenient for trend analysis because trends in extremes at different scales can be analyzed in an easy and universal way through the use of non-stationary GEV distributions ([Marty and Blanchet, 2012, Katz et al., 2002, Westra and Sisson, 2011]).

The goal of this article is to provide a regional evaluation of trend in yearly maxima of daily rainfall in southern France in the recent past (several decades), both at point and spatial scales on a regular grid of $8 \times 8\text{km}^2$. For this, we place ourself in a statistical extreme value framework, which is convenient and theoretically-founded as soon as yearly maxima are concerned. A novelty of this study compared to the litterature in the region ([Norrant and Douguédroit, 2004, Pujol et al., 2007a, Pujol et al., 2007b, Tramblay et al., 2011, Tramblay et al., 2013, Soubeyroux et al., 2015, Vautard et al., 2015]) is that not only local but also areal rainfalls are considered. A difference with [Tramblay et al., 2012] is that here the surface of aggregation is about 10 times smaller than the smallest considered area therein, which enables to study trends at finer space-scales. A second difference is that, unlike in [Pujol et al., 2007a, Pujol et al., 2007b] for example, trends are first assessed locally, which makes possible to reveal the spatial variability of trends and to highlight that the great majority of the significant trends are actually found in quite specific spots. Regional testing is performed in a second step quite similarly to [Pujol et al., 2007b] but focusing on the sub-region where trends are the most significant rather than mixing inhomogeneous trends encountred over the region.

The article is organized as follows. Section 2 presents the data and region of study. Section 3 describes the methodology based on non-stationary GEV distributions. The methodology is neither region- nor scale-specific and could be applied at any space and time scales. Currently it is applied to daily point and areal rainfall on a grid of 8×8 km^2 in southern France. Section 4 discusses the results and a conclusion finishes the article.

2 Studied region and data

The studied region broadly covers the lower basin of the Rhône River (Figure 1). It includes the southeastern edge of the Massif Central towards the West and the first foothills of the Alps towards the East. It is surrounded by the Mediterranean Sea towards the South. The region features a rather flat alluvial plain containing the Rhône delta with on its edges two mountain ridges with elevations reaching between 1500 and 2000m a.s.l. in less than 30 to 50 km. The highest peaks located along the eastern branch of the V-shaped Massif Central mountain (Mounts Aigoual, Lozère, Gerbier de Jonc and Mézenc) are aligned with an orientation of N-30°-E. On the other side of the Rhône Valley, the main peak line is oriented N-160°-E. This funnel-shaped domain is known to experience severe storms generating flash-floods from various foothill rivers. Both sides of the valley can be affected as shown by quite recent severe events causing numerous human losses and considerable damages that occurred in 1992 on the Ouvèze River ([Sénési et al., 1996]) and in 2002 on the Gard River ([Delrieu et al., 2005]). Nevertheless a strong dissymmetry exists in terms of occurrence of such events in this area. The Massif Central edge, called Cévennes-Vivarais region, experiences most of the extreme storms and resulting flash-floods (Figure 2 of [Nuissier et al., 2008]).

This study makes use of both point and areal daily rainfall. Point rainfall stems from a rain-gage network maintained by Météo-France and covering the French administrative departments of Ardèche, Drôme, Gard, Haute-Loire, Herault, Lozère and Vaucluse, with a surface of about $38,000$ km^2 (see Fig. 1). The network covers at most the 1958-2014 period. The SAFRAN database ([Quintana-Seguí et al., 2008]) provides the areal rainfall on a regular grid of 8×8 km^2. It covers the region in 1078 cells (excluding the Mediterranean Sea), see Fig. 1. Daily SAFRAN data are available for the 1958-2013 period, with no missing value. Since flash floods occur in Autumn in this region, we restrict all series to the three months of September, October and November. In order to filter out the point series with too many missing values, the following steps are applied sequentially:

1. For a given station, an autumnal maximum is considered as missing if its rank is smaller than $pmiss \times N$ where $pmiss$ is the proportion of missing values for that autumn, and N is the number of observed autumns.

2. The whole station is excluded from the analysis if less than 20 autumns are missing.

Step 1. in the above procedure is inspired from [Papalexiou and Koutsoyiannis, 2013] but differs in that here the probability to select a maxima is more continuously related to the proportion of missing values. The idea is essentially to consider that an incomplete year with a large proportion of missing values (large $pmiss$) may still have observed the maximum value if that

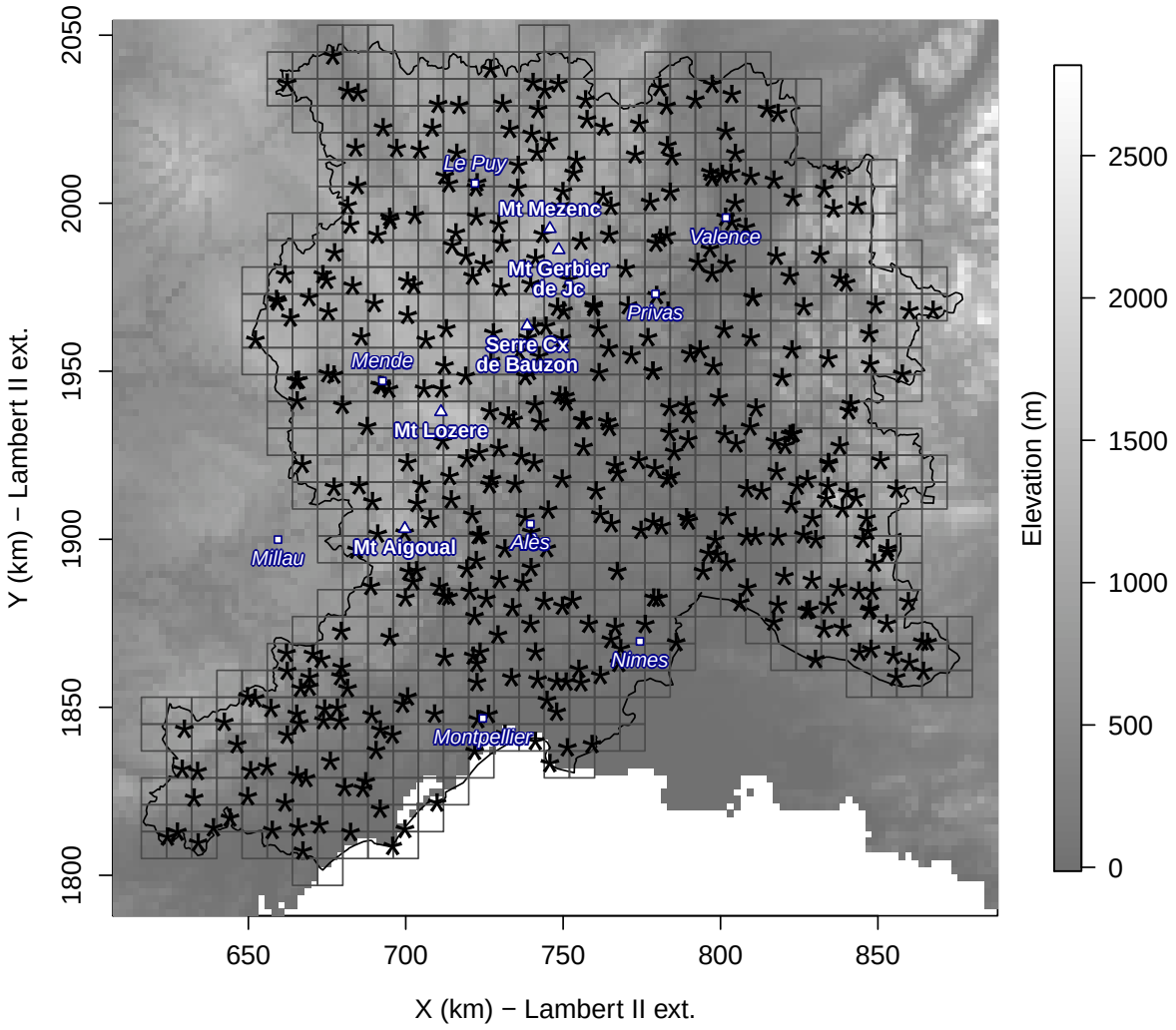

Figure 1: Main features of the region of analysis: elevation above sea level, main mountain peaks (white triangles) and main cities (white squares). Point rainfalls are provided by daily raingages (stars) and areal rainfalls by SAFRAN grids of size 8×8 km^2 (squares). The black border delineates the instrumented area (French administrative departments of Ardèche, Drôme, Gard, Haute-Loire, Hérault, Lozère and Vaucluse).

value is large compared to the other maxima (i.e. its rank is large). Applying this selection procedure, we finally end up with a set of 428 daily point series.

3 Method

3.1 Modeling of maxima

Let R be the random variable of annual maximum rainfall intensity (in mm/h) at a given spatio-temporal scale, and at a given location. We model the statistical distribution of R using the so-called Generalized Extreme Value (GEV) distribution. The reason for this latter choice relies in Extreme Value Theory ([Coles, 2001], chapter 3), which insures that this is the only possible distribution of independent and identically distributed (i.i.d.) maxima. In the stationary case, the cumulative distribution function of R, $\Pr(R \leq r)$, is then given by ([Coles, 2001, Katz et al., 2002]):

$$F(r;\mu,\sigma,\xi) = \begin{cases} \exp\left\{-\left(1+\xi\dfrac{r-\mu}{\sigma}\right)^{-1/\xi}\right\} \text{ if } \xi \neq 0, \text{ provided } 1+\xi\dfrac{r-\mu}{\sigma} > 0, \\ \exp\left\{-\exp\left(-\dfrac{r-\mu}{\sigma}\right)\right\} \text{ if } \xi = 0. \end{cases} \quad (1)$$

Here μ, $\sigma > 0$, and ξ are the location (mm/h), scale (mm/h), and shape (dimensionless) parameters, respectively. Three sub-families of distributions (EV-I, EV-II and EV-III, also known as Gumbel, Fréchet and Reverse Weibull distributions) can be derived from the GEV depending on the sign of its shape parameter, which governs the tail of the distribution. If the shape parameter $\xi > 0$, then the GEV distribution is said to be heavy tailed. This is often the case for rainfall data, in particular in our study area ([Ceresetti et al., 2010]). The case $\xi = 0$ corresponds to the Gumbel case whose distribution is light-tailed. This is also often used in hydrological studies ([Borga et al., 2005]) although there is some evidence that the more general GEV distribution should be preferred ([Papalexiou and Koutsoyiannis, 2013]). The case when $\xi < 0$ is the Reverse Weibull case, corresponding to upper-bounded random variables with upper-end point at $\mu + \sigma/|\xi|$. The case $\xi \leq -0.5$ corresponds to distributions with a very short bounded upper tail, which is unlikely to occur in practice ([Coles, 2001]).

In the non-stationary case, the GEV parameters vary with time (years). In this article, the location parameter is assumed to be a function $\mu(t)$, whilst the scale and shape parameters are constant. Three non-stationary models for $\mu(t)$ are considered:

- A linear trend:

$$\mu(t) = \mu_0 + \mu_1 t, \quad (2)$$

- A linear trend starting in year t_0:

$$\mu(t) = \begin{cases} \mu_0, & t \leq t_0, \\ \mu_0 + \mu_1(t - t_0), & t \geq t_0. \end{cases} \quad (3)$$

- A linear trend before year t_0:

$$\mu(t) = \begin{cases} \mu_0 + \mu_1(t - t_0), & t \leq t_0, \\ \mu_0, & t \geq t_0. \end{cases} \quad (4)$$

The linear case in $\mu(t)$ (Eq. 2) is used in many studies to model non-stationarities in precipitation extremes (e.g. [Katz et al., 2002]). Here we extend this idea by allowing the change to start in some year t_0 (Eq. 3) or to finish in some year t_0 (Eq. 4). [Panthou et al., 2013] uses in West Africa a different model with a jump in t_0, i.e. $\mu(t)$ takes value μ_0 before the change point t_0 and μ_1 after t_0. This induces a discontinuity in the distribution of maxima which seems unrealistic in the region and will not be considered hereafter.

The three above equations involve two unknown parameters for $\mu(t)$, instead of one parameter in the stationary case. This latter case is actually a particular case of Eqs. 2 to 4 under $\mu_1 = 0$. This property will be used in the next section to make trend hypothesis test. The corresponding GEV distribution is obtained by replacing in (1) μ by $\mu(t)$. Since the mean of the GEV distribution is a linear function of μ while its stardard deviation is independent of μ, the mean of annual maxima is expected to experience a linear trend under Eq. 2, or a linear trend with change point under Eqs. 3 and 4, while the standard deviation of the maxima is expected to be constant within the observed period for all models.

Together with the stationary case, four GEV models are thus considered, with respectively three (stationary case) and four (non-stationary case, Eqs. 2 to 4) unknown parameters. These parameters have to be estimated for each series of maxima. In order to insure that enough data are available, we consider:

- the linear case of Eq. 2 for all series having at least 20 years of observations (which is met by all series);
- the linear case with change point in t_0 of Eqs. 3 and 4 for all series having at least 20 years of observations both before and after t_0.

Since the series span over the 1958-2014 period, possible years of change t_0 will be considered between 1977 and 1995. Models of Eqs. 3 and 4 may or may not be considered for a given series, depending on its observation range and on t_0.

All the models are fitted by maximum likelihood ([Coles, 2001], chapter 3.3), independently for each raingage and SAFRAN series. Let consider a given series of n annual maximum intensities, denoted $\mathbf{r} = (r_1, \ldots, r_n)$, and $(t_1, \ldots, t_n)$ the corresponding years. Assuming independence

of annual maxima, the log-likelihood in the non-stationary case is given by

$$\log L(\mu_0, \mu_1, \sigma, \xi) = -n \log(\sigma) - (1 + 1/\xi) \sum_{i=1}^{n} \tilde{r}_i - \sum_{i=1}^{n} \tilde{r}_i^{-1/\xi} \tag{5}$$

where

$$\tilde{r}_i = 1 + \xi \left(\frac{r_i - \mu(t_i)}{\sigma} \right), \tag{6}$$

and $\mu(t)$ is a function of μ_0 and μ_1 as in Eqs. 2, 3 or 4, depending on the considered model. The log-likelihood in the stationary-case is function of (μ_0, σ, ξ) and is also given by Eq. 5, replacing $\mu(t_i)$ by μ_0 in Eq. 6. Denoting θ the three or four GEV parameters, the most likely parameters are those such that $\hat{\theta} = \arg\max_\theta L(\theta)$. Since there is no explicit solution, $\hat{\theta}$ is obtained numerically. Standard errors of the trend μ_1 in the non-stationary models of Eqs. 2 to 4 are obtained from the approximate normality of the maximum likelihood estimator (see [Coles, 2001], chapter 2.6.4) as

$$\mathrm{std}(\hat{\mu}_1) = \sqrt{(I^{-1})_{22}}$$

where $(I^{-1})_{22}$ is the element $(2, 2)$ of the inverse of the observed information matrix I defined by

$$I = \begin{pmatrix} -\frac{\partial^2 \log L(\hat{\theta})}{\partial \mu_0^2} & -\frac{\partial^2 \log L(\hat{\theta})}{\partial \mu_0 \partial \mu_1} & -\frac{\partial^2 \log L(\hat{\theta})}{\partial \mu_0 \partial \sigma} & -\frac{\partial^2 \log L(\hat{\theta})}{\partial \mu_0 \partial \xi} \\ -\frac{\partial^2 \log L(\hat{\theta})}{\partial \mu_0 \partial \mu_1} & -\frac{\partial^2 \log L(\hat{\theta})}{\partial \mu_1^2} & -\frac{\partial^2 \log L(\hat{\theta})}{\partial \mu_1 \partial \sigma} & -\frac{\partial^2 \log L(\hat{\theta})}{\partial \mu_1 \partial \xi} \\ -\frac{\partial^2 \log L(\hat{\theta})}{\partial \mu_0 \partial \sigma} & -\frac{\partial^2 \log L(\hat{\theta})}{\partial \mu_1 \partial \sigma} & -\frac{\partial^2 \log L(\hat{\theta})}{\partial \sigma^2} & -\frac{\partial^2 \log L(\hat{\theta})}{\partial \sigma \partial \xi} \\ -\frac{\partial^2 \log L(\hat{\theta})}{\partial \mu_0 \partial \xi} & -\frac{\partial^2 \log L(\hat{\theta})}{\partial \mu_1 \partial \xi} & -\frac{\partial^2 \log L(\hat{\theta})}{\partial \sigma \partial \xi} & -\frac{\partial^2 \log L(\hat{\theta})}{\partial \xi^2} \end{pmatrix}.$$

3.2 Model selection

Given the estimated models of the previous section, we now wish to decide for each series whether any of the non-stationary model is preferred to the stationary assumption, and if so which one and for which year of change. Here we use GEV likelihood criteria, even for the selection of the best year of change. It has two main advantages over the usual statistical tests relying not on GEV assumptions (see [Beaulieu et al., 2012] for a recent review). First, several studies showed the better performance of the GEV framework when dealing with extreme data ([Katz, 2013, Mallakpour and Villarini, 2015]). Second it allows us to use a common methodological framework throughout all the process of selection of the best non-stationary model, selection of the best year of change, estimation of the trend and testing of trend significance.

In a first step we compare the non-stationary models to one another and select at regional scale which of them give(s) the best model-data fit. Since all considered non-stationary models have four degrees-of-freedom, namely $(\mu_0, \mu_1, \sigma, \xi)$, we can simply compare their likelihoods and select the subset of them giving the highest mean log-likelihood in the region. However,

strictly speaking, this cannot be considered has a regional test for two reasons: first, likelihood comparisons are, strictly speaking, not statistical tests. Second there is spatial dependence among the data and therefore among the likelihoods. This first step can therefore only give evidence about a possible non-stationary model, but not a final decision.

Now let $\mathcal{M}$ be a putative non-stationary model selected at the previous step. In a second step we focus on each series independently. We wish to assess for each of them whether $\mathcal{M}$ should indeed be preferred to the stationary model $\mathcal{M}_0$. First evidence is obtained by comparing the penalized likelihoods under $\mathcal{M}$ and $\mathcal{M}_0$, with a penalization accounting for the difference in degrees-of-freedom between the two models. We use the well-known Akaike and Bayesian Information criteria (respectively AIC, [Akaike, 1974] and BIC, [Schwarz, 1978]), which only differ in the penalizing term. Let $L_{\mathcal{M}}$ and $L_{\mathcal{M}_0}$ be the likelihoods under $\mathcal{M}$ and $\mathcal{M}_0$ (Eq. 5) and $\hat{\theta}$ and $\hat{\theta}_0$ the corresponding most likely parameters. Difference in AIC and BIC between both models is given by:

$$\Delta\text{AIC} = 2\{\log L_{\mathcal{M}}(\hat{\theta}) - \log L_{\mathcal{M}_0}(\hat{\theta}_0)\} - 2 \quad (7)$$

$$\Delta\text{BIC} = 2\{\log L_{\mathcal{M}}(\hat{\theta}) - \log L_{\mathcal{M}_0}(\hat{\theta}_0)\} - \log(n) \quad (8)$$

Positive values of ΔAIC (resp. ΔBIC) gives evidence of preference for the non-stationary model $\mathcal{M}$ rather than $\mathcal{M}_0$. Since our series have length greater than 20 (thus $\log(n) > 2$), BIC penalizes free parameters more strongly than AIC, which tends to favor models with more parameters, especially for small samples ([Wit et al., 2012]). A way to statistically test model $\mathcal{M}$ versus $\mathcal{M}_0$ is to perform a likelihood ratio test (LRT, [Coles, 2001], chapter 2.6). The test applies here because $\mathcal{M}_0$ is a particular case of all considered non-stationary models (corresponding to $\mu_1 = 0$ in Eqs. 2 to 4). Define

$$D = 2\{\log L_{\mathcal{M}}(\hat{\theta}) - \log L_{\mathcal{M}_0}(\hat{\theta}_0)\} \quad (9)$$

to be the deviance statistic. Then, for large n, under the null hypothesis that the series comes from the stationary model $\mathcal{M}_0$ (i.e. $H_0 : \mu_1 = 0$), D should follow a χ^2_1 distribution. Hence, a test of the validity of $\mathcal{M}_0$ relatively to $\mathcal{M}$ at the level of significance α is to reject the stationary model $\mathcal{M}_0$ in favor of $\mathcal{M}$ if D is greater than the $(1-\alpha)$ quantile of the χ^2_1 distribution.

4 Results and Discussion

4.1 Exploratory analysis: spatial features of maxima

This section contextualizes the daily rainfall maxima in the region. More detailed analyzes can be found in [Ceresetti et al., 2012] and [Molinié et al., 2012] for example. Figure 2 maps

the average of maximum intensity (left) and the 95% quantile of maxima (right), both for the point (raingages) and areal (SAFRAN) rainfall data. On average the largest maxima of both point and areal rainfall are found along the Cévennes-Vivarais slope facing South-East. It is interesting to notice that the highest averages of areal rainfall maxima are located over the northern part of the Cévennes-Vivarais slope, around the Serre de la Croix de Bauzon. All along the Cévennes-Vivarais slope, river regularly spaced of about 15km have dug deep valleys. Around the Serre, these secondary valleys are oriented West-East (while Northwest-southeast elsewhere) i.e. perpendicular to the southern mediterranean flux. At this spot, the averages of point and areal rainfall maxima are of the same order of magnitude, i.e. around 6 mm/h accumulated over one day, which is about 140 mm/day. Going more southwest, around Mont Aigoual, the average maximum of areal and point rainfall depart more. Mont Aigoual is well known for experiencing heavy rainfall. The average maximum of point rainfall is similar that of the Serre de la Croix de Bauzon. However, the area around Mont Aigoual is far less prone to heavy rainfall and therefore the maximum of areal rainfall is one third of that of point rainfall. Elsewhere in the study region, areal and point rainfalls are in a good agreement indicating that the homogeneity scale of the average maximum is at least of 8 km.

It is important to keep in mind that the average filters out the variety of events impacting the region. The right panel of Figure 2 intends to illustrate this variety by displaying the 95%-quantile of point and areal rainfall maxima. Again rainfall is quite homogeneous around the Serre de la Croix de Bauzon where the largest point and areal rainfall maxima are similar. The largest point rainfalls are found in the foothills around the town of Alès, which departs from the location of the largest average maxima. In this area, the 95%-quantile of point rainfall maxima is more than twice that of areal rainfall maxima, which illustrates the spatial variability of the largest maxima. The two spots experiencing the largest maxima, namely the foothills around the town of Alès and around the Serre de la Croix de Bauzon, are prone to stationary rainfall. Some processes favoring the stationarity of deep convection over the foothills such as the cold pool have been revealed in [Ducrocq et al., 2008], while [Miniscloux et al., 2001] and [Anquetin et al., 2003] show that the mountain shoulders perpendicular to the atmospheric flow can sustain shallow convection.

4.2 Trend analysis

Now we address the question of whether daily rainfall maxima have exhibited a significant trend in the study region since 1958. A simple way of detecting trends in time series is to fit regression models. However fitting a linear trend on rainfall maxima reveals some weaknesses in terms of robustness due to the high variability of rainfall maxima. Therefore we prefer the use of GEV-

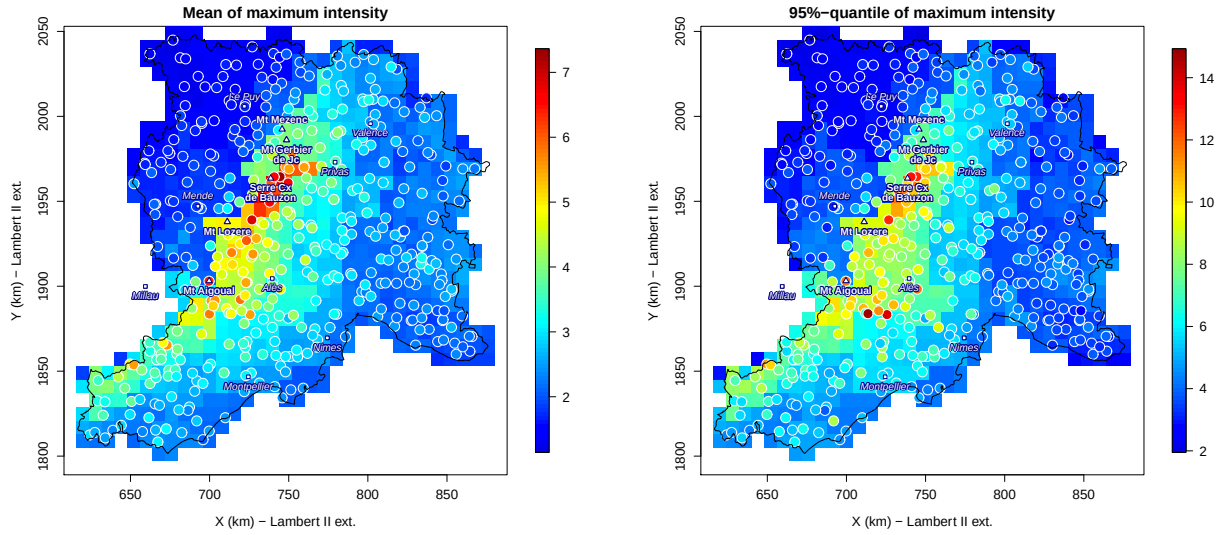

Figure 2: Maps of the daily data. Left: Mean maximum intensity (mm/h). Right: 95%-quantile of maximum intensity (mm/h).

based models (Section 3.1) in order to filter out the seldom occurrence of exceptionally high maxima in the series. An illustration is given by the following robustness analysis. First, we fit to each point series of yearly maxima i) the GEV model of Eq. 1 with linearly varying location parameter (Eq. 2) and ii) a linear regression. Second, we remove the overall maximum of each point series and fit to these new series the two previous models. Figure 3 shows the histograms of the differences in trend estimates, for the two cases. Among the 428 point series, 300 (70%) have an absolute difference smaller than 0.1 mm/day/year in the GEV modeling versus only 184 (43%) when using a regression model, which clearly illustrates a lower sensitivity of the GEV modeling to sampling.

Having selected the GEV-based framework for trend analysis, we now estimate a GEV model to each point and areal series with $\mu(t)$ constrained to vary either linearly (Eq. 2), linearly after a given date t_0 (Eq. 3) or linearly up to a final date t_0 (Eq. 4). We first select which of these non-stationary models fits better the data at regional scale. As explained in Section 3.2, first evidence can be obtained by comparing the mean likelihoods of the different models within the region. Since models of Eqs. 3 and 4 have a change point t_0, which is fixed but unknown, we make estimation of these models by varying t_0 between years 1977 and 1994, in order to insure that 20 years of data are available before the first change point (1977) and after the last one (1994). Figure 4 plots the regional mean of the likelihoods of the non-stationary models, for both point (left) and areal (right) rainfall, as a function of the change point (since the linear model has no change point, it is depicted with horizontal line). In the top of Figure 4 the mean is computed over the stations whose series of maxima has no missing year between 1958 and 2013, which is the observation period of SAFRAN data. Thus each point of Figure 4 is a

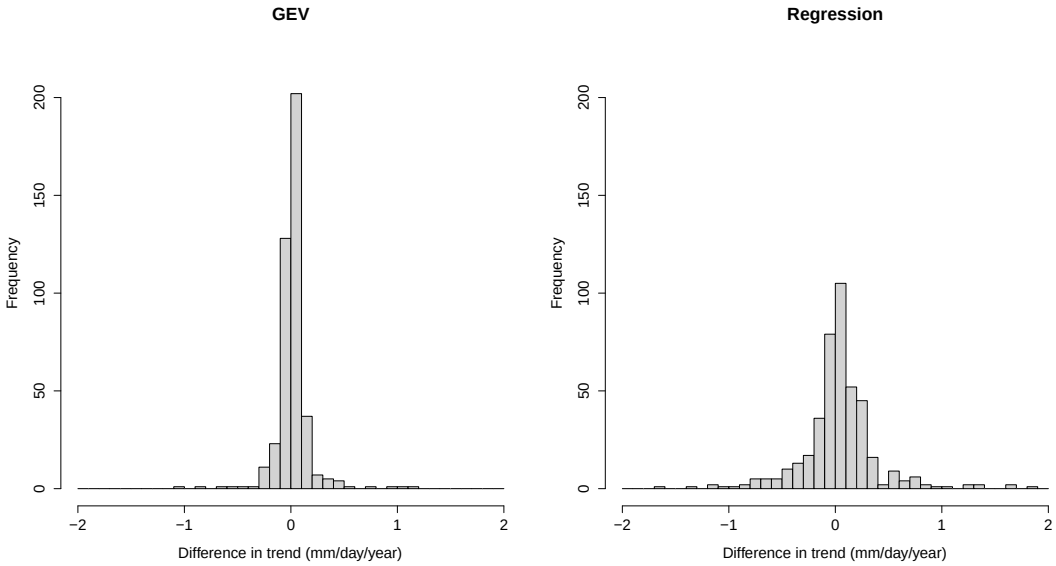

Figure 3: Histogram of difference in trend magnitude (mm/day/year) estimated with and without the overall maximum of each series of yearly point maxima, under either (left) the non-stationary GEV distribution of Eq.2, or (right) a linear regression model.

mean of 88 likelihoods for the point data, and a mean of 682 likelihoods for the areal ones. The same conclusions are drawn from mean log-likelihood comparison in the two cases: whatever the year of change, the model with a recent trend (green line) is more likely than the model with a trend since 1958 (black line), which is itself more likely than a model with a trend in the first subperiod (red line). The best model has a change point in 1985 with a linear trend afterwards. One may be concerned by the fact that the best change point occurs in 1985, which is exactly the center of the observation period. In order to check that there is no bias here, we repeat the same process but we make the GEV estimations on a reduced database starting in 1963 (thus skipping the 5 first years). The bottom of Figure 4 shows that the same conclusion is drawn: at regional scale, the selected model is the non-stationary model of Eq. 3 with a change point in 1985 – which is not anymore the center of the period.

Let stress however that, since rainfall maxima are likely to be spatially correlated over the region ([Bernard et al., 2013]), their joint probability density function is not a product of marginal probabilities, and thus the log-likelihood sum in Figure 4 is not a proper likelihood. Therefore, although Figure 4 gives first insight about some potential starting date of the trend at regional scale, one should keep in mind that this selection criterium relies somehow on an assumption of independence that is unlikely to hold. This assumption is actually made in the large majority of the studies of trends in extremes, including that of [Vautard et al., 2015] for extreme rainfall in the same region, due to the theoretical difficuty in modeling dependence in extremes ([Davison et al., 2012], [Cooley et al., 2012]). A complementary view not relying on

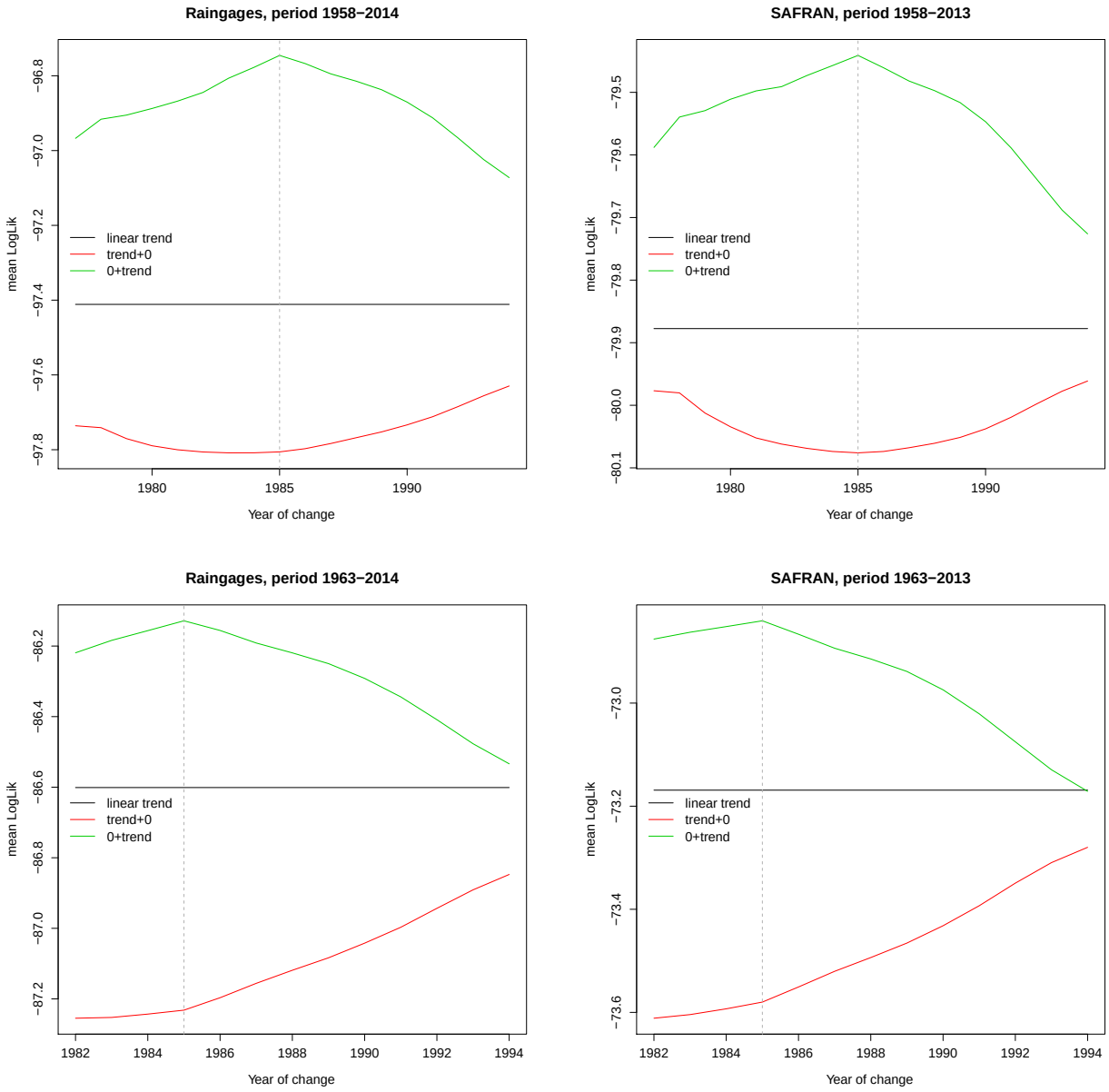

Figure 4: Mean log-likelihood for the three non-stationary models with respect to the year of change for both point (left) and areal (right) rainfall (since the linear model has no change point, it is depicted with horizontal line). Top: for the series with no missing years since 1958. Bottom: for the series with no missing years since 1963.

any regional modeling is obtained by checking for each series independently whether the non-stationary model performs statistically better than the stationary one. Due to its clear better performance compared to the two other considered non-stationary models (see Figure 4), we here focus only on model of Eq. 3 with a trend starting at some date. Figure 5 shows, for each year of change, the percentage of series for which model of Eq. 3 is statistically better than the stationary model. Here we use the selection criteria presented section 3.2, namely AIC and BIC, which are, strictly speaking, not statistical tests but penalized likelihood criteria, and the LRT at levels 5% and 10%, giving in total four criteria per series. Figure 5 reveals a good concordance between the results obtained with AIC and the LRT at level 10% on the one hand (plain lines), and between BIC and the LRT at level 5% on the other hand (dotted lines). Therefore, although they are strictly speaking not statistical tests, AIC and BIC are actually roughly equivalent to likelihood ratio testing. Figure 5 also shows that less trends are detected as significant with BIC than with AIC, which was expected since the former uses a stronger penalization (compare Eq. 7 to 8). The same applies obviously to the two likelihood ratio tests. One finding is that, whatever the criteria, a larger proportion of trends are detected as significant for the point maxima than for the areal ones (compare the blue lines to the red lines). Another finding is that, when using moderately strict tests (in AIC and the LRT at level 10%), all years of changes between the 80's and the 90's seem to be almost as likely, but when the test becomes stricter (in BIC and the LRT at level 5%), the year 1985 pops out as the most likely, which agrees with the results of Figure 4.

Figure 6 maps the series with a significant trend starting in 1985 according to each criterium of Figure 5. The most striking feature is that AIC and the likelihood ratio test at level 10% on one hand, and BIC and the likelihood ratio test at level 5% on the other hand, give the same spatial patterns of trends. So not only the percentage of trends (Figure 5) are similar in each case, but also the same series are detected as non-stationary. Grossly speaking, yearly maxima of daily rainfall over both the Alps and the Cévennes-Vivarais relief, the foothills and the Rhône river valley are likely to vary linearly with time since 1985. This forms a sub-region of exactly half the size the original region where 95% of the significant trends are located (dotted delineation in Figure 6). Furthermore, comparison of point and areal cases in the two maps shows that trends are variable at small-scale. This localized pattern of trends is smoothed out in SAFRAN rainfalls because these are computed as weighted averages of rain-gage series ([Quintana-Seguí et al., 2008, Vidal et al., 2010]) that may exhibit inhomogeneous trends, explaining why less significant trends are found for the areal maxima. Figure 7 shows the magnitude of the estimated trends (left) together with their standard errors (middle) computed following the method of Section 3.1. Most of the study area has undergone an increase in daily

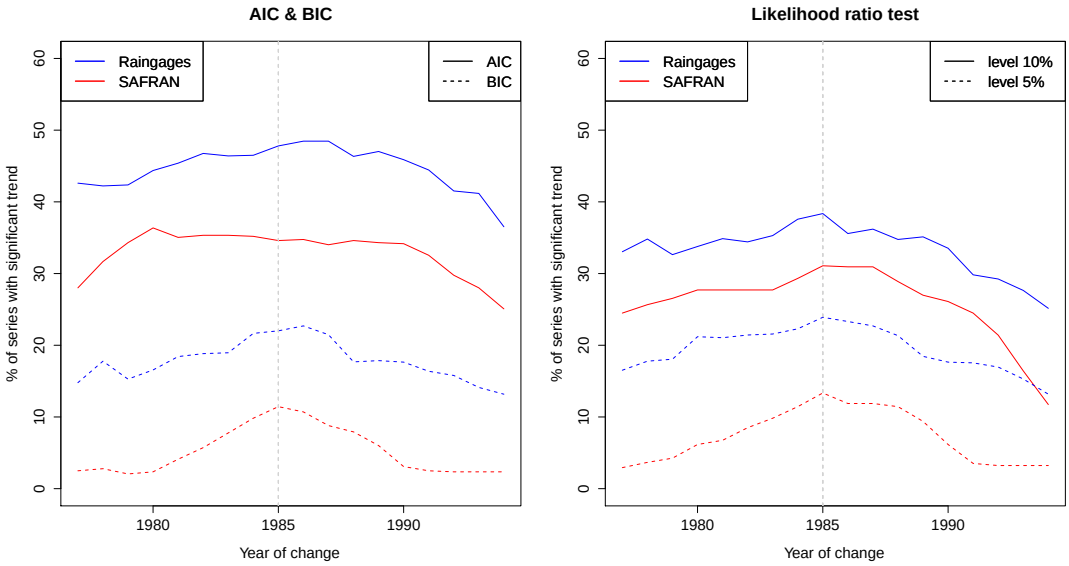

Figure 5: Percentage of series for which the non-stationary GEV distribution of Eq. 3 is preferred to the stationary GEV model of Eq. 1 when the year of change ranges between 1977 and 1994. Preferrence is assessed using AIC (plain-left), BIC (dotted-left) or the likelihood ratio test at levels 10% (plain-right) and 5% (dotted-right).

rainfall maxima since 1985 with larger values in the eastern sub-region where most significant trends are found (see Figure 6). The largest increases of point rainfall maxima are found in two spots: first, along the Cévennes-Vivarais mountain range where increases reach more than 60 mm/day in 20 years. This is however also where uncertainty in the highest, with standard errors around 50% of this increase. Second, around the town of Alès with increases up to about 45 mm/day in 20 years, however again with standard errors of about 50% of this increase. Interestingly, these two spots feature respectively the largest averages and the largest absolute values of rainfall maxima (see Fig. 2). The largest trends in areal rainfall maxima are found in the whole Cévennes-Vivarais slope with up to 1.5 mm/day/year increase. This area features also the largest averages of yearly areal maxima (see Fig. 2). Thus, whatever point or areal rainfall, the largest trends are found where rainfall maxima are the largest. This is however In order to filter out this effect, we display in the right panel of Figure 7 the trend magnitudes relatively to the averages of rainfall maxima. The same two spots, around Alès and the Cévennes-Vivarais slope, still feature among the largest relative trends with increases in the last 20 years reaching up to 40% of the average maxima in these areas. Few other spots stand out: the southwest of the region, which is prone to heavy rainfall events when southeasterly low level flux is blocked by the Pyrenees mountains at the South and by the Massif Central at the North, sustaining deep convection ([Ducrocq et al., 2008, Duffourg and Ducrocq, 2011]); the coastal region of Montpellier and the northern part of the Rhône river valley around the town of Valence. There, the

Vercors and Massif Central mountains are closed (about 20 km) drawing a strait where flows the Rhône river. This topography may block southerly air mass flux. [Froidurot et al., 2015] notices that 3-hourly rainfall is considerable in this area and features a marked diurnal cycle. One possible mechanism is the influence of the sea breeze which can penetrate inland up to Valence ([Bastin et al., 2005, Drobinski et al., 2006]) and which has been associated to rain in other coastal areas ([Pielke, 1974, Hill et al., 2010]). On the other hand, the mountainous areas south of the Massif Central or the area west of Montpellier have experienced very little increase, if not decrease, in the last 20 years (see Fig. 7). This high variability of trends shows that complex physical processes play a role in the occurrence of trends in the region.

The previous results show significance of local trends. Still remains the question: is the number of trends detected in Figure 6 significant *at regional scale*? Answering this question belongs to the domain of field significance. If the maxima were independent, then field significance could be obtained either by comparing the distribution of the local test p-values to the uniform distribution ([Vogel and Kroll, 1989]), or of the number of rejection of local tests to the binomial distribution ([Livezey and Chen, 1983]), or by considering the regional likelihood as a sum of local likelihoods and applying any test of non-stationarity, e.g. LRT, possibily correcting for the effective degrees of freedom due to spatially dependent trends ([Bretherton et al., 1999, Vautard et al., 2015]). However, applying these tests in our case would be inconsistent owing to the spatial dependence of rainfall maxima ([Bernard et al., 2013]). It would tend to an overestimation of the regional p-value and thus an underestimation of the Type I error rate. Thus, properly testing field significance requires taking into account the spatial correlation among maxima: is the number of trends detected in Figure 6 significant at regional scale, given the spatial correlation of the rainfall maxima? We address this question by a bootstrap procedure ([Douglas et al., 2000, Renard et al., 2008, Pujol et al., 2007b]), which is an iterative simulation procedure allowing to empirically estimate the distribution of the number of locally significant trends under the null hypothesis that the series of maxima are stationary but spatially correlated. We use 1000 bootstrap runs. Each run consists of the following steps ([Renard et al., 2008]): (i) Sample the years with replacement and create the new database obtained by replacing the original series of maxima by the maxima corresponding to these bootstrapped years; (ii) Apply the four tests of Figure 6 to each bootstrapped series; (iii) Maps the series with significant trends as in Figure 6. In the end, 1000 maps such as those of Figure 6 are obtained. Comparing the number of significant trends in the original maps of Figure 6 to the bootstrapped maps gives an approximate p-value of the test of field significance, estimated as the proportion of the bootstrapped maps showing more significant trends than Figure 6. Table 1 shows these p-values depending on the database, on the criterium for local testing and on

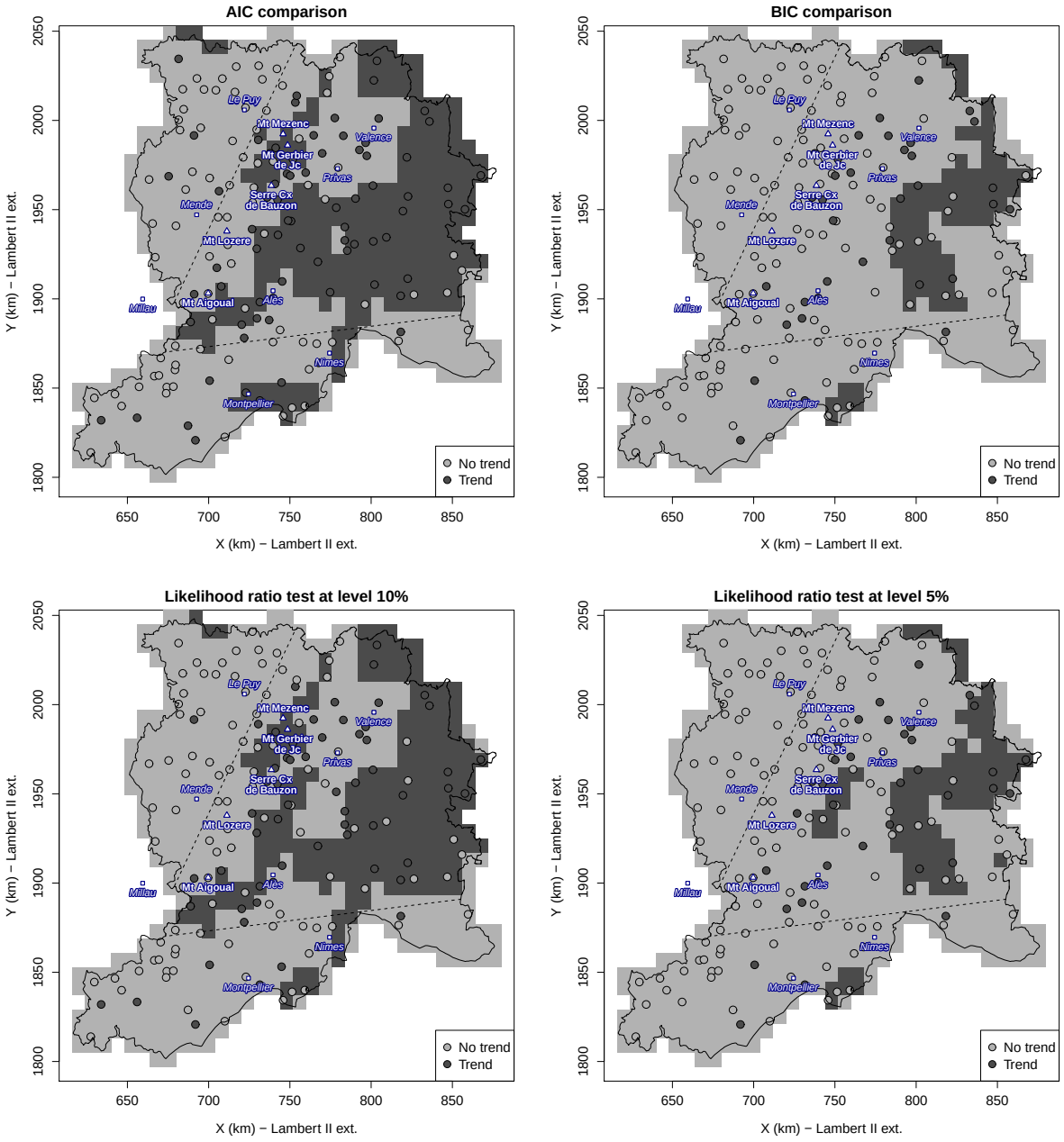

Figure 6: Test of trend at daily scale. The considered non-stationary model is that of Eq. 3 with a change in 1985. Preferrence is assessed using AIC (top-left), BIC (top-right) or the likelihood ratio test at levels 10% (bottom-left) and 5% (bottom-right). The dotted lines delineate the border of the eastern sub-region where the large majority of the significant trends are found.

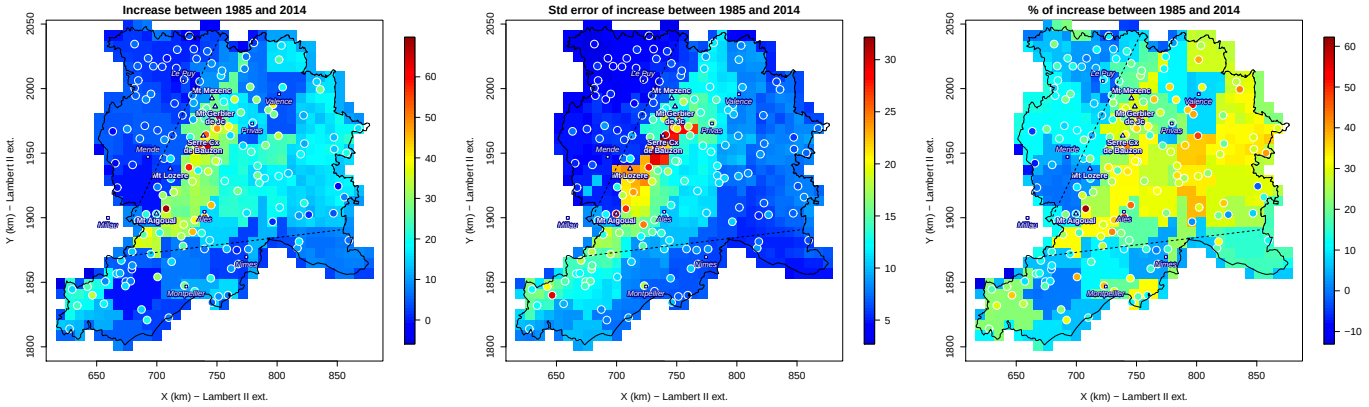

Figure 7: Trend in yearly maxima of daily rainfall accumulation between 1985 and 2014. Left: Magnitude of increase (mm/day). Middle: Standard error of increase (mm/day). Right: Percentage of increase with respect to the average maxima of the series. The dotted lines delineate the border of the eastern sub-region where the large majority of the significant trends are found.

		AIC	BIC	LRT 10%	LRT 5%
whole region	Raingages	3.5 **	4.3 **	2.8 **	4.2 **
eastern region	Raingages	2.3 **	3.2 **	2.2 **	3 **
whole region	SAFRAN	13.4	17	8.8 *	16
eastern region	SAFRAN	6.5 *	10 *	3.6 **	9.1 *

Table 1: Proportion (%) of the bootstrap runs detecting more significant trends than those detected on the orginal data, when considering either the whole region or the eastern part. The criteria to detect trends are AIC, BIC and LRT at levels 10% and 5%. Very significant trends at regional scale are shown with ** (p-value smaller that 5%), moderately significant trend with * (p-value between 5% and 10%).

the considered region. Point rainfall maxima show highly positive trends at the regional scale with all criteria (first row of Table 1), whereas areal rainfalls are moderately significant with a LRT at level 10% and non significant otherwise (third row). When restricting to the eastern sub-region where the large majority of the significant trends are (see Figure 6), trends in point rainfall maxima become even more significant (second row) and trends in areal maxima become all significant, and even very significant with a LRT at level 10% (fourth row).

5 Conclusion

This study addresses trends in yearly maxima of daily point and areal rainfall in southern France. The adopted methodology is to model the statistical distribution of rainfall maxima by different cases of non-stationary GEV models in which the location parameter changes linearly

with years either after or before a given date. Such non-stationary models assume a translation of the distribution of maxima from year to year towards higher or lower values, before or after a given date. The stationary model is a particular case when the linear trend is null. The proposed methodology for trend analysis involves three steps. First, all the considered non-stationary models are estimated for each point and areal rainfall series of maxima. Second, the best model is selected at regional scale by likelihood comparisons, which also allows us to select the best trend-starting/ending date. Third the corresponding non-stationary model is objectively tested for each series of maxima to assess significance of the trends, both at local and regional scales.

This statistical framework is applied to 52 years of both point and areal rainfall data on 8×8 km^2 grids in southern France. The results show a fairly good accordance of the detected trends for the two spatial scales. At regional scale, the most likely starting date of the trend lies between the 80's and the 90's, with 1985 as the most likely. The trend in point rainfall is highly significantly positive in half the region including most of the mountain ranges and part of the Rhône valley. Spatial rainfall also indicates positive trends in these area, however usually of lower magnitude and thus of lower significance. In terms of trend magnitude, two spots stand particularly out for the two spatial scales: the Cévennes-Vivarais ridge and around Alès. These two spots feature both the largest rainfall maxima and the largest trends, which can reach an increase in yearly maxima of more than 62 mm/day in 20 years. This is considerable since it represents more than 40% of the average maximum in this area. Such a high relative increase occurs also in areas where maxima are rather moderate, such as the Rhone river valley, while the mountainous region south of the Massif Central and the area west of Montpellier have experienced very little increase, if not decrease.

These results question the processes leading to trends. How are these results in agreement with the well-known Clausius-Clapeyron relationship? If the atmosphere contains more precipitable water due to global warming, why does it imprint rainfall maxima in some regions and not in others? Insights on the amount of precipitable water (e.g. [Duffourg and Ducrocq, 2011]) are necessary to understand the occurrence of trends. However the question of rainfall sampling is of primary importance. Better understanding may be gained by analysing trends in sub-daily rainfall maxima, which are less prone to stationary precipitation ([Ceresetti et al., 2010, Molinié et al., 2012]). Unfortunately such chronological rainfall series are usually neither long enough nor dense enough to provide reliable statistics at regional scale.

References

[Akaike, 1974] Akaike, H. (1974). A new look at the statistical model identification. *Automatic Control, IEEE Transactions on*, 19(6):716–723.

[Alexander et al., 2006] Alexander, L. V., Zhang, X., Peterson, T. C., Caesar, J., Gleason, B., Klein Tank, A. M. G., Haylock, M., Collins, D., Trewin, B., Rahimzadeh, F., Tagipour, A., Rupa Kumar, K., Revadekar, J., Griffiths, G., Vincent, L., Stephenson, D. B., Burn, J., Aguilar, E., Brunet, M., Taylor, M., New, M., Zhai, P., Rusticucci, M., and Vazquez-Aguirre, J. L. (2006). Global observed changes in daily climate extremes of temperature and precipitation. *Journal of Geophysical Research: Atmospheres*, 111(D5):n/a–n/a.

[Alpert et al., 2002] Alpert, P., Ben-Gai, T., Baharad, A., Benjamini, Y., Yekutieli, D., Colacino, M., Diodato, L., Ramis, C., Homar, V., Romero, R., Michaelides, S., and Manes, A. (2002). The paradoxical increase of Mediterranean extreme daily rainfall in spite of decrease in total values. *Geophysical Research Letters*, 29(11):31–1–31–4.

[Anquetin et al., 2003] Anquetin, S., Miniscloux, F., and Creutin, J. D. (2003). Numerical simulation of orographic rainbands. *J. Geoph. Res.*, 108(D8).

[Bastin et al., 2005] Bastin, S., Drobinski, P., Dabas, A., Delville, P., Reitebuch, O., and Werner, C. (2005). Impact of the Rhône and Durance valleys on sea-breeze circulation in the Marseille area. *Atmospheric Research*, 74(1-4):303–328.

[Beaulieu et al., 2012] Beaulieu, C., Chen, J., and Sarmiento, J. L. (2012). Change-point analysis as a tool to detect abrupt climate variations. *Philosophical Transactions of the Royal Society of London A: Mathematical, Physical and Engineering Sciences*, 370(1962):1228–1249.

[Bernard et al., 2013] Bernard, E., Naveau, P., Vrac, M., and Mestre, O. (2013). Clustering of maxima: spatial dependencies among heavy rainfall in France. *Journal of climate*, (26):7929–7937.

[Blanchet et al., 2015] Blanchet, J., Ceresetti, D., Molinié, G., and Creutin, J.-D. (2015). A regional GEV scale-invariant framework for Intensity - Duration - Frequency analysis. *Submitted*.

[Borga et al., 2005] Borga, M., Vezzani, C., and Fontana, G. D. (2005). Regional Rainfall Depth-Duration-Frequency Equations for an Alpine Region. *Natural Hazards*, 36(1-2):221–235.

[Bretherton et al., 1999] Bretherton, C. S., Widmann, M., Dymnikov, V. P., Wallace, J. M., and Bladé, I. (1999). The effective number of spatial degrees of freedom of a time-varying field. *Journal of Climate*, 12:1990–2009.

[Ceresetti et al., 2010] Ceresetti, D., Molinié, G., and Creutin, J.-D. (2010). Scaling properties of heavy rainfall at short duration: A regional analysis. *Water Resources Research*, 46(9).

[Ceresetti et al., 2012] Ceresetti, D., Ursu, E., Carreau, J., Anquetin, S., Creutin, J. D., Gardes, L., Girard, S., and Molinié, G. (2012). Evaluation of classical spatial-analysis schemes of extreme rainfall. *Nat. Hazards Earth Syst. Sci.*, 12:3229–3240.

[Charney et al., 1979] Charney, J., Arakawa, A., Baker, D., Bolin, B., Dickenson, R., Goody, R., Leith, C., Stommel, H., and Wunsch, C. (1979). Carbon dioxide and climate: A scientific assessment. *National Academy of Sciences Press*, page 33.

[Coles, 2001] Coles, S. (2001). *An introduction to statistical modeling of extreme values*. Springer Series in Statistics. Springer-Verlag, London.

[Cooley et al., 2012] Cooley, D., Cisewski, J., Erhardt, R. J., Jeon, S., Mannshardt, E., Omolo, B. O., and Sun, Y. (2012). A survey of spatial extremes: Measuring spatial dependence and modeling spatial effects. *REVSTAT*, 10(1):135–165.

[Davison et al., 2012] Davison, A. C., Padoan, S. A., and Ribatet, M. (2012). Statistical Modeling of Spatial Extremes. *Statistical Science*, 27(2):161–186.

[Delrieu et al., 2005] Delrieu, G., Nicol, J., Yates, E., Kirstetter, P.-E., Creutin, J.-D., Anquetin, S., Obled, C., and Saulnier, G.-M. (2005). The Catastrophic Flash-Flood Event of 8-9 September 2002 in the Gard Region, France: A First Case Study for the Cévennes-Vivarais Mediterranean Hydrometeorological Observatory. *Journal of Hydrometeorology*, 6:34–52.

[Douglas et al., 2000] Douglas, E., Vogel, R., and Kroll, C. (2000). Trends in floods and low flows in the United States: impact of spatial correlation. *Journal of Hydrology*, 240(1-2):90–105.

[Drobinski et al., 2006] Drobinski, P., Bastin, S., Dabas, A., Delville, P., and Reitebuch, O. (2006). Variability of three-dimensional sea breeze structure in southern France: observations and evaluation of empirical scaling laws. *Annales Geophysicae*, 24(7):1783–1799.

[Ducrocq et al., 2008] Ducrocq, V., Nuissier, O., Ricard, D., Lebeaupin, C., and Thouvenin, T. (2008). A numerical study of three catastrophic precipitating events over western mediterranean region (Southern France): Part II: Mesoscale triggering ans stationarity factors. *Quart. J. Roy. Meteor. Soc.*, 134(630):131–145.

[Duffourg and Ducrocq, 2011] Duffourg, F. and Ducrocq, V. (2011). Origin of the moisture feeding the heavy precipitating systems over southeastern France. *Nat. Hazards Earth Syst. Sci*, 11(4):1163–1178.

[Fabry, 1996] Fabry, F. (1996). On the determination of scale ranges for precipitation fields. *Journal of Geophysical Research: Atmospheres*, 101(D8):12819–12826.

[Fraedrich and Larnder, 1993] Fraedrich, K. and Larnder, C. (1993). Scaling regimes of rainfall time series. *Tellus*, 45A:289–298.

[Frich et al., 2002] Frich, P., Alexander, L. V., Della-Marta, P., Gleason, B., Haylock, M., Klein Tank, A., and Peterson, T. (2002). Observed coherent changes in climatic extremes during the second half of the twentieth century. *Climate Research*, 19:193–212.

[Froidurot et al., 2015] Froidurot, S., Molinié, G., and Diedhiou, A. (2015). Rainfall in Southeast France at the Regional Climate Model scales. *submitted to the Med-CORDEX special issue of Climate Dynamics*.

[Gallant et al., 2013] Gallant, A. J. E., Karoly, D. J., and Gleason, K. L. (2013). Consistent Trends in a Modified Climate Extremes Index in the United States, Europe, and Australia. *Journal of Climate*, 27(4):1379–1394.

[Gupta and Waymire, 1979] Gupta, V. and Waymire, E. (1979). A Stochastic Kinematic Study of Subsynoptic Space-Time Rainfall. *Water Resources Research*, 15(3):637–644.

[Haylock and Goodess, 2004] Haylock, M. R. and Goodess, C. M. (2004). Interannual variability of European extreme winter rainfall and links with mean large-scale circulation. *International Journal of Climatology*, 24(6):759–776.

[Hill et al., 2010] Hill, C. M., Fitzpatrick, P. J., Corbin, J. H., Lau, Y. H., and Bhate, S. K. (2010). Summertime Precipitation Regimes Associated with the Sea Breeze and Land Breeze in Southern Mississippi and Eastern Louisiana. *Weather and Forecasting*, 25(6):1755–1779.

[IPCC, 2013] IPCC (2013). *Climate Change 2013: The Physical Science Basis. Contribution of Working Group I to the Fifth Assessment Report of the Intergovernmental Panel on Climate Change*. Cambridge University Press, Cambridge, United Kingdom and New York, NY, USA.

[Karl et al., 1996] Karl, T. R., Knight, R. W., Easterling, D. R., and Quayle, R. G. (1996). Indices of Climate Change for the United States. *Bull. Amer. Meteor. Soc.*, 77(2):279–292.

[Katz, 2013] Katz, R. W. (2013). *Extremes in a Changing Climate: Detection, Analysis and Uncertainty*, chapter Statistical Methods for Nonstationary Extremes, pages 15–37. Springer Netherlands, Dordrecht.

[Katz et al., 2002] Katz, R. W., Parlange, M. B., and Naveau, P. (2002). Statistics of extremes in hydrology. *Advances in Water Resources*, 25(8-12):1287–1304.

[Klein Tank and Können, 2003] Klein Tank, A. M. G. and Können, G. P. (2003). Trends in Indices of Daily Temperature and Precipitation Extremes in Europe, 1946-99. *J. Climate*, 16(22):3665–3680.

[Livezey and Chen, 1983] Livezey, R. E. and Chen, W. Y. (1983). Statistical field significance and its determination by monte carlo techniques. *Monthly Weather Review*, 111:46–59.

[Mallakpour and Villarini, 2015] Mallakpour, I. and Villarini, G. (2015). A simulation study to examine the sensitivity of the Pettitt test to detect abrupt changes in mean. *Hydrological Sciences Journal*, 0(0):1–10.

[Marty and Blanchet, 2012] Marty, C. and Blanchet, J. (2012). Long-term changes in annual maximum snow depth and snowfall in Switzerland based on extreme value statistics. *Climatic Change*, 111(3-4):705–721.

[Miniscloux et al., 2001] Miniscloux, F., Creutin, J. D., and Anquetin, S. (2001). Geostatistical analysis of orographic rainbands. *J. Appl. Meteorol.*, 40:1835–1854.

[Molinié et al., 2012] Molinié, G., Ceresetti, D., Anquetin, S., Creutin, J. D., and Boudevillain, B. (2012). Rainfall regime of a mountainous mediterranean region: statistical analysis at short time steps. *Journal of Applied Meteorology and Climatology*, 51(3):429–448.

[Norrant and Douguédroit, 2004] Norrant, C. and Douguédroit, A. (2004). Tendances des précipitations mensuelles et quotidiennes dans le Sud-Est méditerranéen français (1950-51 /1999-2000). *Annales de l'association internationale de climatologie*, 1:45–64.

[Nuissier et al., 2008] Nuissier, O., Ducrocq, V., Ricard, D., Lebeaupin, C., and Anquetin, S. (2008). A numerical study of three catastrophic precipitating events over western mediterranean region (Southern France): Part I: Numerical framework and synoptic ingredients. *Quart. J. Roy. Meteor. Soc.*, 134(630):111–130.

[Panthou et al., 2013] Panthou, G., Vischel, T., Lebel, T., Quantin, G., Pugin, A.-C. F., Blanchet, J., and Ali, A. (2013). From pointwise testing to a regional vision: An integrated statistical approach to detect nonstationarity in extreme daily rainfall. Application to the Sahelian region. *Journal of Geophysical Research: Atmospheres*, 118(15):8222–8237.

[Papalexiou and Koutsoyiannis, 2013] Papalexiou, S. M. and Koutsoyiannis, D. (2013). Battle of extreme value distributions: A global survey on extreme daily rainfall. *Water Resources Research*, 49(1):187–201.

[Pielke, 1974] Pielke, R. A. (1974). A Three-Dimensional Numerical Model of the Sea Breezes Over South Florida. *Monthly Weather Review*, 102(2):115–139.

[Planton et al., 2008] Planton, S., Déqué, M., Chauvin, F., and Terray, L. (2008). Expected impacts of climate change on extreme climate events. *Comptes Rendus Geoscience*, 340(9-10):564 – 574.

[Pujol et al., 2007a] Pujol, N., Neppel, L., and Sabatier, R. (2007a). Approche régionale pour la détection de tendances dans des séries de précipitations de la région méditerranéenne française. *Comptes Rendus Geoscience*, 339(10):651 – 658.

[Pujol et al., 2007b] Pujol, N., Neppel, L., and Sabatier, R. (2007b). Regional tests for trend detection in maximum precipitation series in the French Mediterranean region. *Hydrological Sciences Journal/Journal des Sciences Hydrologiques*.

[Quintana-Seguí et al., 2008] Quintana-Seguí, P., Le Moigne, P., Durand, Y., Martin, E., Habets, F., Baillon, M., Canellas, C., Franchisteguy, L., and Morel, S. (2008). Analysis of Near-Surface Atmospheric Variables: Validation of the SAFRAN Analysis over France. *Journal of Applied Meteorology and Climatology*, 47(1):92–107.

[Ramos et al., 2005] Ramos, M. H., Creutin, J.-D., and Leblois, E. (2005). Visualization of storm severity. *Journal of Hydrology*, 315(1–4):295 – 307.

[Renard et al., 2008] Renard, B., Lang, M., Bois, P., Dupeyrat, A., Mestre, O., Niel, H., Sauquet, E., Prudhomme, C., Parey, S., Paquet, E., Neppel, L., and Gailhard, J. (2008). Regional methods for trend detection: Assessing field significance and regional consistency. *Water Resources Research*, 44(8):n/a–n/a. W08419.

[Schertzer and Lovejoy, 1987] Schertzer, D. and Lovejoy, S. (1987). Physically based rain and cloud modeling by anisotropic, multiplicative turbulent cascades. *Journal of Geophysical Research*, 92:9692–9714.

[Schmidli and Frei, 2005] Schmidli, J. and Frei, C. (2005). Trends of heavy precipitation and wet and dry spells in Switzerland during the 20th century. *International Journal of Climatology*, 25(6):753–771.

[Schwarz, 1978] Schwarz, G. (1978). Estimating the Dimension of a Model. *The Annals of Statistics*, 6(2):461–464.

[Sénési et al., 1996] Sénési, S., Bougeault, P., Chèze, J.-L., Cosentino, P., and Thepenier, R.-M. (1996). 1996: The vaison-la-romaine flash flood: mesoscale analysis and predictability issues. *Weather and Forecasting*, 11(4):417–442.

[Soubeyroux et al., 2015] Soubeyroux, J.-M., Neppel, L., Veysseire, J.-M., Tramblay, Y., Carreau, J., and Gouget, V. (2015). Evolution des précipitations extrêmes en France en contexte de changement climatique. *La Houille Blanche*, (1):27–33.

[Toreti et al., 2010] Toreti, A., Xoplaki, E., Maraun, D., Kuglitsch, F. G., Wanner, H., and Luterbacher, J. (2010). Characterisation of extreme winter precipitation in Mediterranean coastal sites and associated anomalous atmospheric circulation patterns. *Natural Hazards and Earth System Sciences*, 10(5):1037–1050.

[Tramblay et al., 2011] Tramblay, Y., Neppel, L., and Carreau, J. (2011). Climatic covariates for the frequency analysis of heavy rainfall events in the Mediterranean region. *Natural Hazards and Earth System Sciences*, 11(9):2463–2468.

[Tramblay et al., 2013] Tramblay, Y., Neppel, L., Carreau, J., and Najib, K. (2013). Non-stationary frequency analysis of heavy rainfall events in Southern France. *Hydrological Sciences Journal - Journal des Sciences Hydrologiques*, 58(2):280–294.

[Tramblay et al., 2012] Tramblay, Y., Neppel, L., Carreau, J., and Sanchez-Gomez, E. (2012). Extreme value modelling of daily areal rainfall over Mediterranean catchments in a changing climate. *Hydrological processes*, 26(25):3934–3944.

[Vautard et al., 2015] Vautard, R., van Oldenborgh, G.-J., S. Thao, B. D., Lenderink, G., Ribes, A., Planton, S., Soubeyroux, J.-M., and Yiou, P. (2015). Extreme fall 2014 precipitation in the Cévennes mountains. *Bulletin of the American Meteorological Society*, 96(12).

[Vidal et al., 2010] Vidal, J.-P., Martin, E., Franchistéguy, L., Baillon, M., and Soubeyroux, J.-M. (2010). A 50-year high-resolution atmospheric reanalysis over France with the Safran system. *International Journal of Climatology*, 30(11):1627–1644.

[Vogel and Kroll, 1989] Vogel, R. and Kroll, C. (1989). Low-flow frequency analysis using probability plot correlation coefficients. *Journal of Water Resources Planning and Management*, 115(3):338–357.

[Westra and Sisson, 2011] Westra, S. and Sisson, S. A. (2011). Detection of non-stationarity in precipitation extremes using a max-stable process model. *Journal of Hydrology*, 406(1–2):119–128.

[Wit et al., 2012] Wit, E., Heuvel, E. v. d., and Romeijn, J.-W. (2012). 'All models are wrong...': an introduction to model uncertainty. *Statistica Neerlandica*, 66(3):217–236.

[Zhang et al., 2011] Zhang, X., Alexander, L., Hegerl, G. C., Jones, P., Tank, A. K., Peterson, T. C., Trewin, B., and Zwiers, F. W. (2011). Indices for monitoring changes in extremes

based on daily temperature and precipitation data. *Wiley Interdisciplinary Reviews: Climate Change*, 2(6):851–870.

[Zolina, 2014] Zolina, O. (2014). Multidecadal trends in the duration of wet spells and associated intensity of precipitation as revealed by a very dense observational German network. *Environmental Research Letters*, 9(2):025003.

[Zolina et al., 2008] Zolina, O., Simmer, C., Kapala, A., Bachner, S., Gulev, S., and Maechel, H. (2008). Seasonally dependent changes of precipitation extremes over Germany since 1950 from a very dense observational network. *Journal of Geophysical Research: Atmospheres*, 113(D6):n/a–n/a.